Early alterations in myocardia and vessels of the diabetic rat heart: an FTIR microspectroscopic study

Neslihan TOYRAN*[1], Peter LASCH†, Dieter NAUMANN†, Belma TURAN‡ and Feride SEVERCAN*[2]

*Department of Biological Sciences, Middle East Technical University, 06531 Ankara, Turkey, †P25-Biomedical Spectroscopy, Robert Koch-Institut, Nordufer 20, D-13353 Berlin, Germany, and ‡Department of Biophysics, Faculty of Medicine, Ankara University, 06100 Ankara, Turkey

Diabetes mellitus is associated with a high incidence and poor prognosis of cardiovascular disease. The aim of the present study was to examine the effect of relatively short-term (5 weeks) Type I diabetes on the left ventricle, the right ventricle and the vessel (vein) on the left ventricle of the myocardium at molecular level by FTIR (Fourier-transform infrared) microspectroscopy. The rats were categorized into two groups: control group (for the left ventricle myocardium, $n = 8$; for the right ventricle myocardium, $n = 9$; for the vein, $n = 9$) and streptozotocin-induced diabetic group (for the left ventricle myocardium, $n = 7$; for the right ventricle myocardium, $n = 9$; for the vein, $n = 8$). Two adjacent cross-sections of 9 μm thickness were taken from the ventricles of the hearts in two groups of rats by using a cryotome. The first sections were used for FTIR microspectroscopy measurements. The second serial sections were stained by haematoxylin/eosin for comparative purposes. Diabetes caused an increase in the content of lipids, an alteration in protein profile with a decrease in α-helix and an increase in β-sheet structure as well as an increase in glycogen and glycolipid contents in both ventricles and the vein. Additionally, the collagen content was found to be increased in the vein of the diabetic group. The present study demonstrated that diabetes-induced alterations in the rat heart can be detected by correlating the IR spectral changes with biochemical profiles in detail. The present study for the first time demonstrated the diabetes-induced alterations at molecular level in both ventricle myocardia and the veins in relatively short-term diabetes.

Key words: Fourier-transform infrared (FTIR), microscopy, myocardium, Type I diabetes, vein, ventricle.

INTRODUCTION

Diabetes mellitus (DM) is defined as a disorder of carbohydrate metabolism caused by absence or deficiency of insulin, insulin resistance or both, ultimately leading to a cluster of disorders. This disease is associated with an extensive list of complications involving many organs: the cardiovascular system (atherosclerosis and macro- and micro-angiopathies) [1], central and peripheral nervous system (neuropathy) [2], eyes (cataract and blindness) [3], kidneys (renal failure) [4] and liver (hepatomegaly) [5].

With the development of effective treatments for the infectious, metabolic and renal complications of DM, cardiovascular disease now looms as the most dreaded complication. Among the complications of diabetes, cardiovascular disease is the leading cause of death in diabetic patients [6]. Long-standing diabetes has been documented to cause structural and functional cardiac impairment and to lead to ischaemic heart disease, cardiomyopathy and congestive heart failure [7]. It was found in a previous study that structural changes in patients with diabetes were associated with impaired ventricular performance [7]. Over 8 and 16 weeks of diabetes, the left ventricular myocardium of the diabetic rats sustained damage that was progressively more serious with the duration of the diabetic state [8]. In rats exposed to 8 weeks of diabetes, the myocardium contained large numbers of lipid droplets and glycogen granules around mitochondria, which showed patchy swelling and slight loss of myofilaments [8]. Most clinical studies of diabetic heart failure have the marked diminution of ventricular function [9], which is characterized by impairment of left ventricular relaxation and systolic performance [10]. In a previous study, haemodynamic and echocardiographic measurements showed thickening of the wall and an increase in the internal dimension of the left ventricle in STZ (streptozotocin)-induced diabetic rats at week 8 [11]. These changes were even more pronounced in rats after 12 weeks of STZ application. Furthermore, the authors of the same study noted an increase in collagen in the diabetic hearts [11]. The number of studies concerning the effect of diabetes on the right ventricle is rather limited, possibly because the pathological processes are expected to primarily involve the myocardium of the left ventricle. In one of the studies performed on the right ventricle, there was experimental evidence that the right ventricle in rats was affected more seriously than the left one. The degree of right ventricular necrosis and fibrosis of hypertensive diabetic rats paralleled that in the left ventricle, but was unexpectedly several times greater in magnitude [12].

Type I DM often leads to coronary atherosclerosis related to hypertriglyceridaemia and altered lipoprotein profiles, resulting in vascular insufficiency, ischaemia and a markedly increased risk of myocardial infarction [13]. Small-vessel coronary artery disease frequently occurs in diabetic patients [14]. However, the role of small-vessel disease in the pathophysiology of cardiomyopathy remains unclear. In a previous study, it was suggested based on necropsy findings that changes in the small vessels of the myocardium are responsible for diabetic cardiomyopathy [15]. In another study, it was reported that diabetic patients have an increased sensitivity to catecholamines, which may cause

Abbreviations used: AGE, advanced glycation end-product; DM, diabetes mellitus; FTIR, Fourier-transform infrared; FWHH, full width at half height; H/E, haematoxylin/eosin; STZ, streptozotocin.

[1] Present address: Department of Physiology, Faculty of Medicine, Baskent University, 06530 Ankara, Turkey.
[2] To whom correspondence should be addressed (email feride@metu.edu.tr).

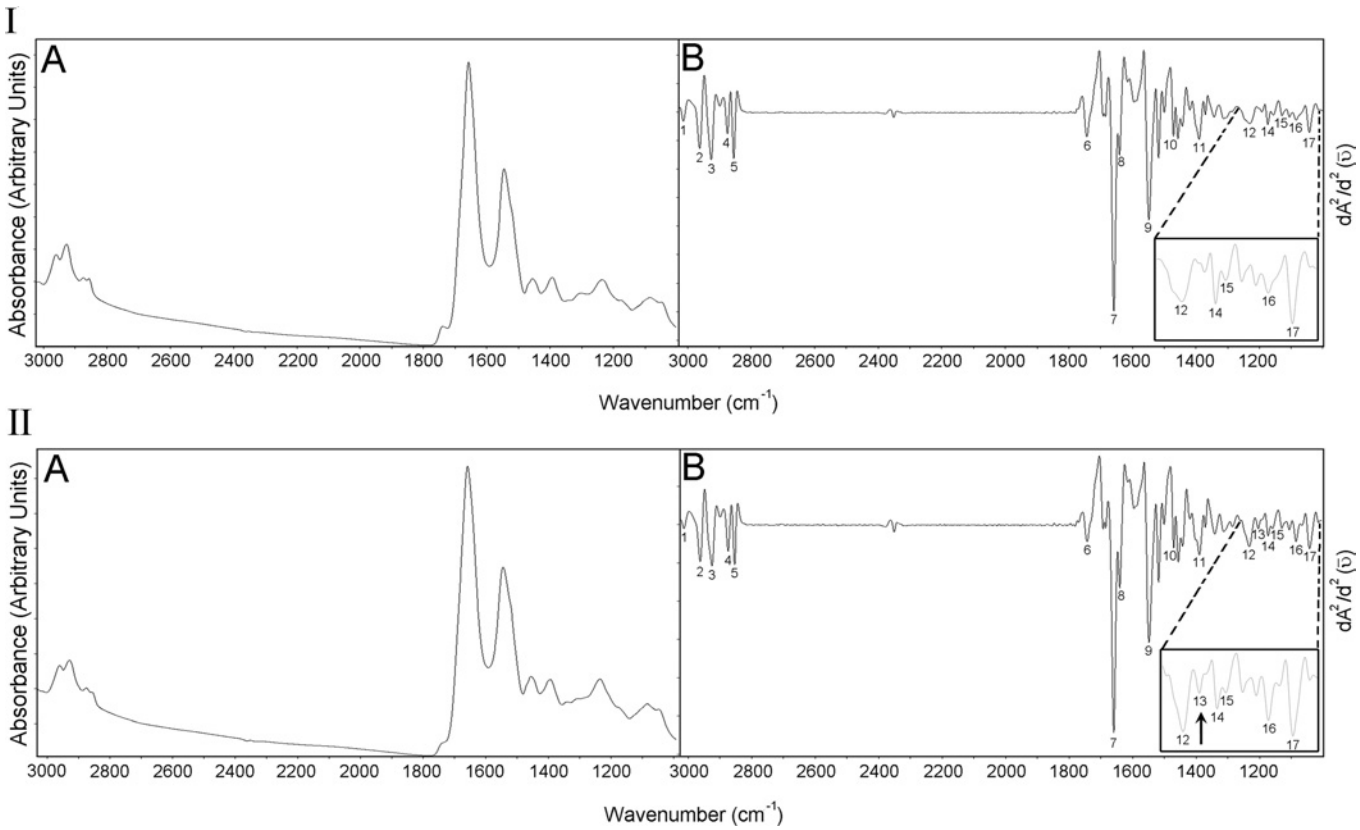

Figure 1 Absorption (IA) and second derivative (IB) spectra of the control left ventricle myocardium; absorption (IIA) and second derivative (IIB) spectra of the control vein

Enlarged form of the spectra, in 1000–1270 cm^{-1} regions, are shown on the right sides of the Figures displaying the second derivatives. Absorption maxima appear as minima in the second derivatives.

myocardial ischaemia by focal small coronary artery vasoconstriction [16]. A variety of pathological lesions of the small, intramural arterioles, capillaries and venules have been described in the diabetic heart. Ultrastructural studies have demonstrated a significant increase in the thickening of the basement membranes of small blood vessels in the diabetic heart [17]. The relative contributions of these lesions to the pathogenesis of diabetic heart disease are still unknown.

Taking into consideration these results, we aimed to investigate the effects of short-term (5 weeks) DM on the myocardia and small veins of the diabetic heart. Due to its structural and conformational sensitivity, FTIR (Fourier-transform infrared) microspectroscopy was found to be an ideal tool for a comparative study. IR spectroscopy is a widely used method for analysing molecular structure and structural interactions in biological systems. It measures absorption of vibrating molecules that have resulted from the energy transitions of vibrating dipoles. Very small alterations in bond lengths and angles can be detected by this technique and therefore it has emerged as a powerful tool to investigate the structural changes in the molecules in detail. Very rapid advances in the applications of IR spectroscopy to the study of biological molecules have occurred with the development of sophisticated FTIR spectrometers. Despite the fact that the same information was obtained from the spectra recorded with dispersive instruments (IR) and interferometers (FTIR), the FTIR technique enables the rapid and reproducible recording of high-resolution, low-noise spectra even in aqueous medium. The data acquisition process is automated. The data obtained are stored in

Table 1 Band assignments of major absorptions in IR spectra of heart tissue in 3300–1000 cm^{-1} region

Peak numbers of this Table are illustrated in Figure 1.

Peak numbers	Frequency (cm^{-1})	Assignments
1	3012	Olefinic=CH stretching: unsaturated lipids [24,28]
2	2956	CH_3 asymmetric stretching: lipids [23,49]
3	2925	CH_2 asymmetric stretching: lipids [32]
4	2873	CH_3 symmetric stretching: mainly proteins [50]
5	2854	CH_2 symmetric stretching: lipids [50]
6	1733–1739	C=O stretching: ester functional groups in lipids [23]
7	1655	Amide I: (mainly protein C=O stretching), α-helical structure [24]
8	1638	Amide I: β-sheet [24]
9	1545	Amide II: (protein N–H bending, C–N stretching), α-helical structure [24]
10	1468	CH_2 scissoring: lipids [50]
11	1386	CH_3 bending: lipids [29]
12	1228	PO_2^- asymmetric stretching: phospholipids, nucleic acids [45]
13	1201	Collagen [24]
14	1173	CO–O–C asymmetric stretching: ester bonds in cholesteryl esters [29]
15	1156	C–O stretching: glycogen, nucleic acids [45]
16	1080–1085	PO_2^- symmetric stretching: phospholipids, nucleic acids [45] C–O stretching: glycogen, oligosaccharides, glycolipids [29,32]
17	1041	C–O stretching: oligosaccharides, polysaccharides [33]

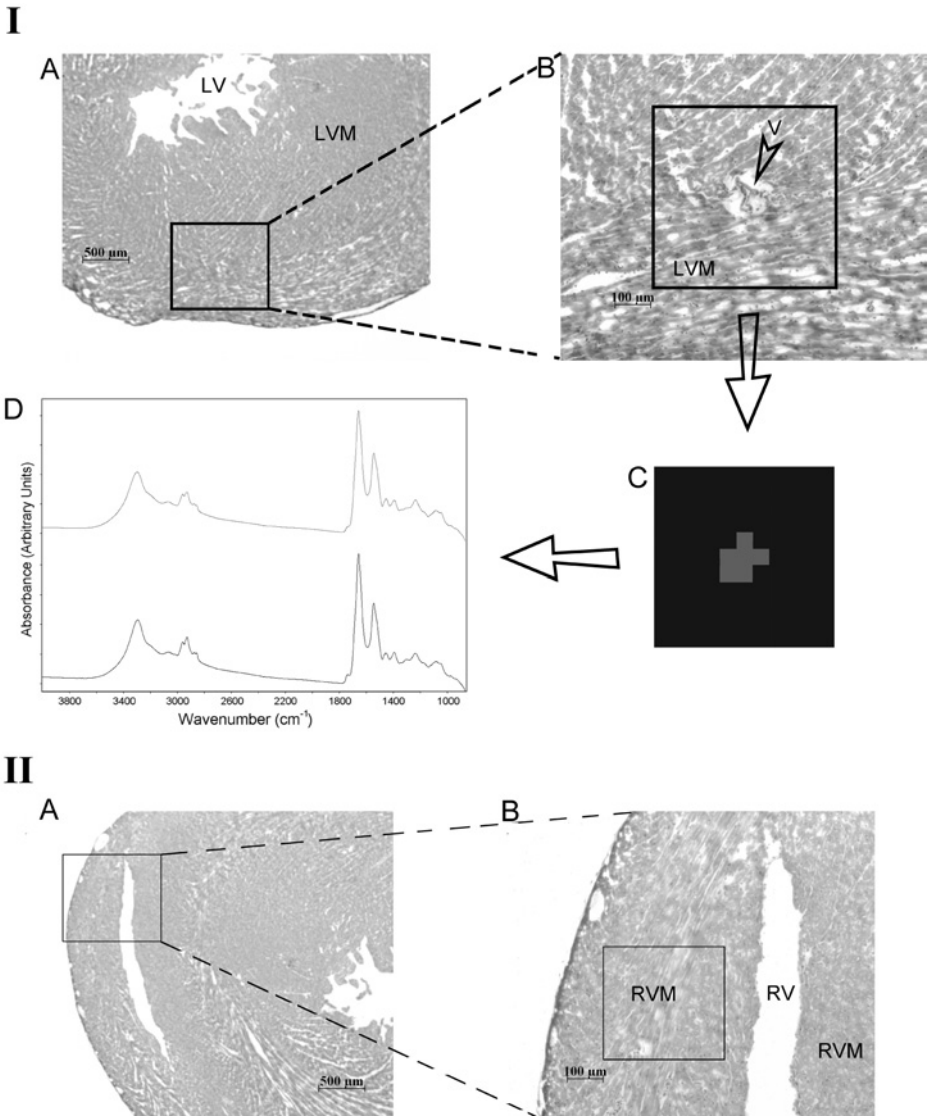

Figure 2 Light microscope images and mapped regions of the rat heart

(**IA**) Light microscope image of H/E-stained thin slice taken from the left ventricle at $\times 25$ magnification. (**IB**) The mapped region of the left ventricle myocardium at $\times 100$ magnification. (**IC**) The image of cluster analysis in 950–1480 cm^{-1} region. (**ID**) The average spectrum arising from different clusters. (**IIA**) Light microscope image of H/E-stained thin slice taken from the right ventricle of rat heart at $\times 25$ magnification. (**IIB**) The same image including the mapped region at $\times 100$ magnification. Abbreviations: LV, left ventricle; LVM, left ventricle myocardium; V, vein; RV, right ventricle; RVM, right ventricle myocardium.

digitally encoded formats, which facilitates spectral interpretation with the aid of post-acquisition data manipulation algorithms. This property of the technique provides the accurate detection of small changes even in the weak absorption bands [18].

IR microspectroscopy is the combination of IR spectroscopy and microscopy which is exceptionally well suited for differentiating distinct tissue structures and identifying tissue pathology. It is a powerful technique that can be used to collect IR spectra from microscopic regions of tissue sections to reveal chemical and physical changes. These changes can provide insights into the biochemical and biophysical mechanisms of disease processes [19–21]. Furthermore, with this technique, it is possible to overcome some of the restrictions introduced by homogenization and/or extraction of the sample to be analysed [22].

MATERIALS AND METHODS

Experimental animals

Male and female adult Wistar rats (Animal Care Facility, Faculty of Medicine, Ankara University), ranging from 200 to 250 g body weight, were selected randomly. They were housed in stainless-steel, wire-bottomed cages, initially at a density of three per cage and as they grew, they were caged individually. They were maintained at a 12 h light/dark cycle and an ambient air temperature of 22 ± 1 °C. All the experimental procedures used in the present study were approved by the Ethics Committee of Ankara University, Faculty of Medicine. Rats were divided into two groups: control group (for the left ventricle myocardium, $n = 8$; for the right ventricle myocardium, $n = 9$; for the vein, $n = 9$) and STZ-induced diabetic group (for the left ventricle

myocardium, $n = 7$; for the right ventricle myocardium, $n = 9$; for the vein, $n = 8$).

Control group

The blood glucose levels of the randomly chosen rats were measured. Afterwards, a single dose of 0.1 M citrate buffer (pH 4.5) was injected intraperitonally. The rats were fed without any restriction. The glucose levels were measured every week for a 5 week period following the injections. The rats were anaesthetized by pentobarbital (30 mg/kg; Sigma). To remove the hearts, the rats were killed by opening their chest. Then the removed hearts were stored at $-80\,^{\circ}C$ for experimental analysis.

STZ-induced diabetic group

STZ, an antibiotic causing a sustained insulin deficiency and an elevation of serum glucose levels by selectively destroying pancreatic β-cells, was used to induce Type I DM in the experimental animals of the present study. Citrate buffer (0.1 M; pH 4.5) was used to dissolve STZ (Sigma). The dissolved STZ was injected intraperitoneally as a single dose at a concentration of 50 mg/kg body weight. Blood glucose levels were measured 1 week after the STZ injection. Rats that had a blood glucose level of higher than three times the control value were accepted as diabetic. Rats with blood glucose levels less than three times the control value were excluded from the study. Feeding, anaesthesia and heart removal were carried out in the same way as for the animals of the control group.

IR mapping experiments and data acquisition

Two adjacent cross-sections of 9 μm thickness were taken from the ventricles of all the groups by using cryotome and were thaw-mounted on IR-transparent CaF_2 windows. A small amount of optimum cutting tool was applied to tissue samples to allow the sample to be attached to the cryotome. The first sections taken from all the samples were used for FTIR microspectroscopy measurements. The tissue samples were stored at room temperature (25 °C) in a desiccator filled with nitrogen gas. For comparison by light microscopy, the second serial sections were routinely stained by H/E (haematoxylin/eosin). A region in the left ventricle myocardium including a vein (~ 100 μm in diameter) and a region in the right ventricle myocardium were mapped.

An IR microscope coupled with an IFS28B FTIR spectrometer (both from Bruker, Germany) was used to map the tissue sections. The microscope was equipped with a computer-controlled x/y stage that permitted spectral mapping of the tissue in defined steps within a rectangular area. A grid of pixel coordinates within the tissue section was defined and IR spectra were collected from each of the points in the grid. Spectra were taken in both the x- and y-directions in steps of 56 μm, using a circular aperture 70 μm in diameter. In this way, IR data completely covering the chosen tissue area could be obtained. IR spectra were collected as absorbance spectra from 850 to 4000 cm^{-1} with a spectral resolution of 6 cm^{-1} using a mercury–cadmium–telluride detector. The number of co-added interferograms per spectrum was set to 256. The microscope, which was hermetically sealed using a specially designed box, and the spectrometer were purged with dry air to reduce spectral contributions from water vapour and CO_2. We used all the tissue sections from both groups for the IR mapping and data processing.

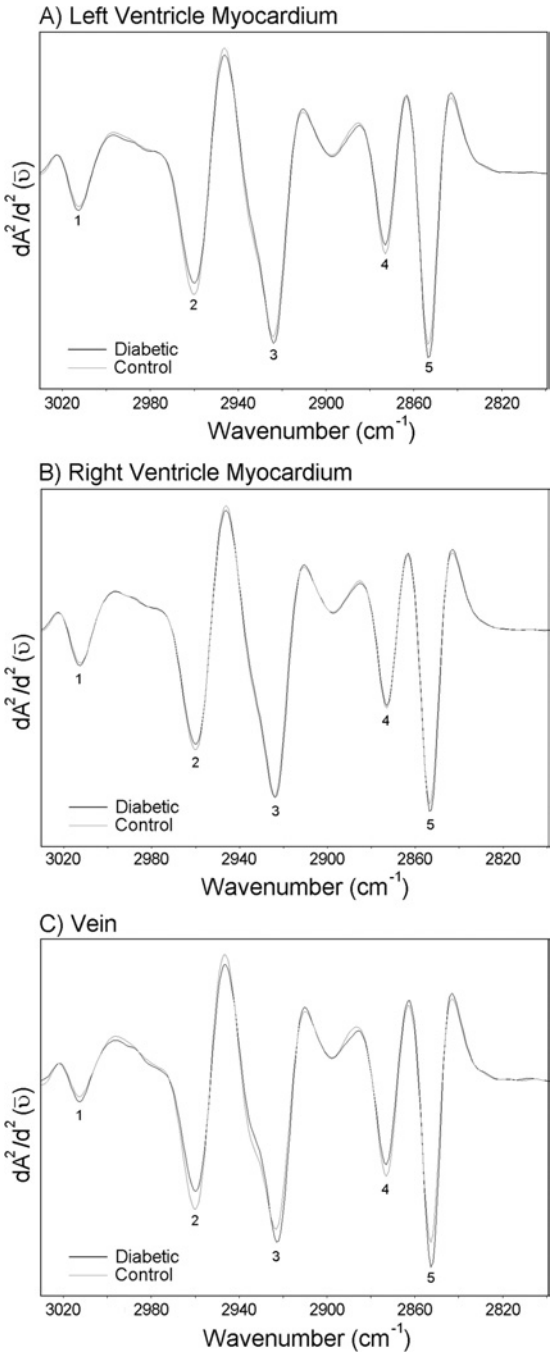

Figure 3 Average spectra belonging to the left ventricle myocardium, the right ventricle myocardium and the vein of the control and the diabetic groups in the 2800–3030 cm^{-1} region

Vector normalization was done in the 2800–3050 cm^{-1} region. Absorption maxima appear as minima in the second derivatives. (**A**) Second derivative average spectra belonging to the left ventricle myocardium; (**B**) second derivative average spectra belonging to the right ventricle myocardium; (**C**) second derivative average spectra belonging to the vein.

IR data evaluation

Quality tests, first derivative calculations, vector normalizations, cluster analysis and spectra averaging were performed using a program, written by Peter Lasch, which is now available from CytoSpec (http://www.cytospec.com). Further analysis of spectral data was carried out using the OPUS^{NT} data collection software package (Bruker Optics, Reinstetten, Germany).

Table 2 Changes in the intensities of the main functional groups in the 2800–3030 cm^{-1} region for control and diabetic groups

Data are given as means ± S.D. $P \leqslant 0.05$ were accepted as significantly different from the control group.

	Left ventricle myocardium			Right ventricle myocardium			Vein		
Functional groups	Control	Diabetic	*P* values	Control	Diabetic	*P* values	Control	Diabetic	*P* values
CH_3 asym. stretching (at 2956 cm^{-1})	−0.118 ± 0.005	−0.105 ± 0.002	⩽0.001	−0.116 ± 0.004	−0.108 ± 0.003	⩽0.01	−0.127 ± 0.006	−0.109 ± 0.004	⩽0.001
CH_2 asym. stretching- (at 2925 cm^{-1})	0.172 ± 0.003	−0.178 ± 0.003	⩽0.01	−0.174 ± 0.002	−0.174 ± 0.003		−0.150 ± 0.007	−0.169 ± 0.006	⩽0.01
CH_3 sym. stretching (at 2873 cm^{-1})	−0.085 ± 0.002	−0.075 ± 0.002	⩽0.001	−0.082 ± 0.002	−0.079 ± 0.002		−0.100 ± 0.004	−0.090 ± 0.007	⩽0.01
CH_2 sym. stretching (at 2854 cm^{-1})	−0.184 ± 0.002	−0.198 ± 0.004	⩽0.001	−0.185 ± 0.003	−0.190 ± 0.002	⩽0.001	−0.170 ± 0.004	−0.200 ± 0.012	⩽0.001

Table 3 Changes in lipid/protein ratio for control and diabetic groups

Data are given as means ± S.D. $P \leqslant 0.05$ were accepted as significantly different from the control group.

	Left ventricle myocardium			Right ventricle myocardium			Vein		
Parameter	Control	Diabetic	*P* values	Control	Diabetic	*P* values	Control	Diabetic	*P* values
Lipid/protein ratio	1.20 ± 0.05	1.28 ± 0.09	⩽0.05	1.09 ± 0.06	1.18 ± 0.05	⩽0.01	1.06 ± 0.04	1.15 ± 0.06	⩽0.01

First steps of data evaluation included a so-called 'quality test' of the raw spectral data. Quality tests were carried out as described previously [23].

All spectra passing the quality test were subsequently converted into first derivatives in the 950–1480 and 2800–3050 cm^{-1} spectral regions using a five-smoothing point Savitzky–Golay algorithm. Then the first derivatives were normalized in the frequency range of 950–1480 cm^{-1}. Cluster analysis (hierarchical clustering) was performed on the first derivative spectra in the 950–1480 and 2800–3050 cm^{-1} regions. Cluster analysis gives information on spectral relationships or on spectral similarity. In the present study, cluster analysis was used for the identification of tissue structures. Similar spectra from defined tissue structures (e.g. veins and myocardium) were identified by the use of cluster analysis and averaged afterwards to have a better signal/noise ratio, and better representation of certain tissue biochemistry/composition. The cluster analysis was performed for only the left ventricle to distinguish between the left ventricle myocardium and the vein on the left ventricle myocardium. For the right ventricle myocardium, cluster analysis was not performed, because there was no other structure on the mapped region of all the rat hearts to be distinguished. The original absorption spectra and their averages belonging to different clusters were saved in a format readable by $OPUS^{NT}$. Then the data were loaded into $OPUS^{NT}$.

Since most IR bands are broad and composed of overlapping components, direct comparisons of spectral characteristics were performed on normalized second derivatives of average spectra of the discussed spectral classes. Absorption spectra were used only for the analysis of the lipid/protein ratio by calculating the integrals between 2820–3050 cm^{-1} (for the lipid content) and 1620–1690 cm^{-1} (for the protein content). For comparisons between the control and diabetic groups, the second derivative spectra were vector normalized at 2800–3050 cm^{-1} (for the comparisons made in the 2800–3030 cm^{-1} region) and at 950–1480 cm^{-1} (for the comparisons made in the 1480–1800 and 1000–1480 cm^{-1} regions). The second derivative of the original spectra offers a direct way to identify the peak frequencies of characteristic components and thus permits much more detailed qualitative and, eventually, quantitative studies. Then, the averages of the individuals belonging to the same group were calculated. The same procedure was applied for all the control and diabetic groups and the resultant average spectra were compared. Absorption maxima appear as minima in the second derivatives. For this reason, minimum positions were used for the comparisons in the second derivative spectra. In the second derivative spectra, peak height is very sensitive to changes of FWHH (full width at half height) of the IR bands. However, cells and tissues are composed of similar substances, which cause broad and superimposed IR bands. We assumed that the FWHH does not exhibit significant changes over certain cellular structures and therefore, in the present study, second-order derivative spectra were used to monitor concentration-sensitive changes, as reported by others [24–26].

Statistics

The results were expressed as means ± S.D. The differences in the means for the diabetic and control rats were compared by means of Mann–Whitney U test. *P* values equal to or less than 0.05 were accepted as significantly different from the control group. The degree of significance was denoted as: $^{*}P \leqslant 0.05$, $^{**}P \leqslant 0.01$, $^{***}P \leqslant 0.001$. The statistical analyses on Tables 1–5 are from many mappings belonging to heart tissues and veins of all rats.

RESULTS

Absorption and the second derivative spectra of the left ventricle myocardium from control group are given in Figures 1(IA) and 1(IB) respectively. Control right ventricle myocardium has a very similar spectrum to left ventricle myocardium (results not shown). Absorption and second derivative spectra of control vein is shown in Figures 1(IIA) and 1(IIB) respectively. Both the left and the right ventricle myocardia have almost the same absorption bands.

However, a new band appears at approx. 1201 cm^{-1} [pointed with an arrow in Figure 1(IIB)] in the vein spectra. Some important absorption bands of the IR spectra are labelled in Figures 1(IB) and 1(IIB), and the band assignments are given in Table 1.

The FTIR results are analysed for the following spectral regions: 2800–3030, 1480–1800 and 1000–1480 cm^{-1}.

Figure 2(IA) shows a light microscope image of an H/E-stained specimen taken from the left ventricle of the rat heart at $\times 25$ magnification. The mapped region of the left ventricle myocardium is shown at $\times 100$ magnification in Figure 2(IB). The cluster image and the average spectra arising from different clusters are shown in Figures 2(IC) and 2(ID) respectively. The basis of image assembly in cluster analysis is to assign a distinct colour to all spectra in one cluster. In Figures 2(IC) and 2(ID), it is possible to see two different clusters represented by two different colours belonging to different tissue components and the original average absorption spectra of these clusters respectively. The grey colour arises from the vein and the black colour arises from the left ventricle myocardium. The corresponding original average absorption spectra are shown with the same corresponding colours. The aim of this cluster analysis is to distinguish between the signals coming from the vein and the left ventricle myocardium. The cluster analysis was performed for all the rat hearts.

Figure 2(IIA) shows a light microscope image of an H/E-stained section taken from the right ventricle of rat heart at $\times 25$ magnification. The same image including the mapped region is given in Figure 2(IIB) at $\times 100$ magnification.

The 2800–3030 cm^{-1} region

Between 2800 and 3030 cm^{-1}, spectral features are dominated by absorption bands of the asymmetric and symmetric C–H stretching vibrations of CH_2 and CH_3 methylene groups contained in fatty acids in cellular membranes. A weak band near 3012 cm^{-1} is also observed, resulting from the C–H stretching vibrations of =C–H groups in unsaturated fatty acids [23]. Average derivative spectra belonging to the left ventricle myocardium, the right ventricle myocardium and the vein of the control and the diabetic groups are given in Figure 3. The changes in the intensities of main functional groups are given in Table 2. As seen in Figure 3 and Table 2, the changes observed between the control and diabetic groups in this region are quite similar for all the investigated regions of the heart. The intensities of the CH_2 asymmetric and the symmetric stretching modes increase in the diabetic groups, more significantly in the left ventricle myocardium and the vein. As demonstrated in Figure 3 and Table 2, the intensities of the CH_3 symmetric and the asymmetric stretching bands decrease in the diabetic groups. Figure 3 also reveals that the intensity of the band at approx. 3012 cm^{-1} increases significantly only in the vein of the diabetic group with respect to the control (from -0.017 ± 0.006 to $-0.023 \pm 0.005^{*}$). The intensity of this band did not change significantly in the left or right ventricle myocardia. Table 3 shows the changes in lipid/protein ratio. It is observed that this ratio increases significantly in all the investigated regions of the diabetic heart with respect to the control.

The 1480–1800 cm^{-1} region

The region between 1500 and 1800 cm^{-1} is dominated by the conformation-sensitive Amide I and Amide II bands, which can be used to discriminate between the protein secondary structures α-helix and β-pleated sheet [27]. The average spectra belonging to the left ventricle myocardium, the right ventricle myocardium and the vein of the control and the diabetic groups in the 1480–1800 cm^{-1} region are given in Figure 4. The changes in the intensities of main functional groups are given in Table 4. Since the peak maximum of the Amide I band occurs at different frequencies for various types of hydrogen-bonded secondary structures, the discrete types of secondary structure in proteins can be identified by the frequencies of their maxima in the FTIR spectra [28]. The band at 1655 cm^{-1} is attributable to Amide I of α-helical

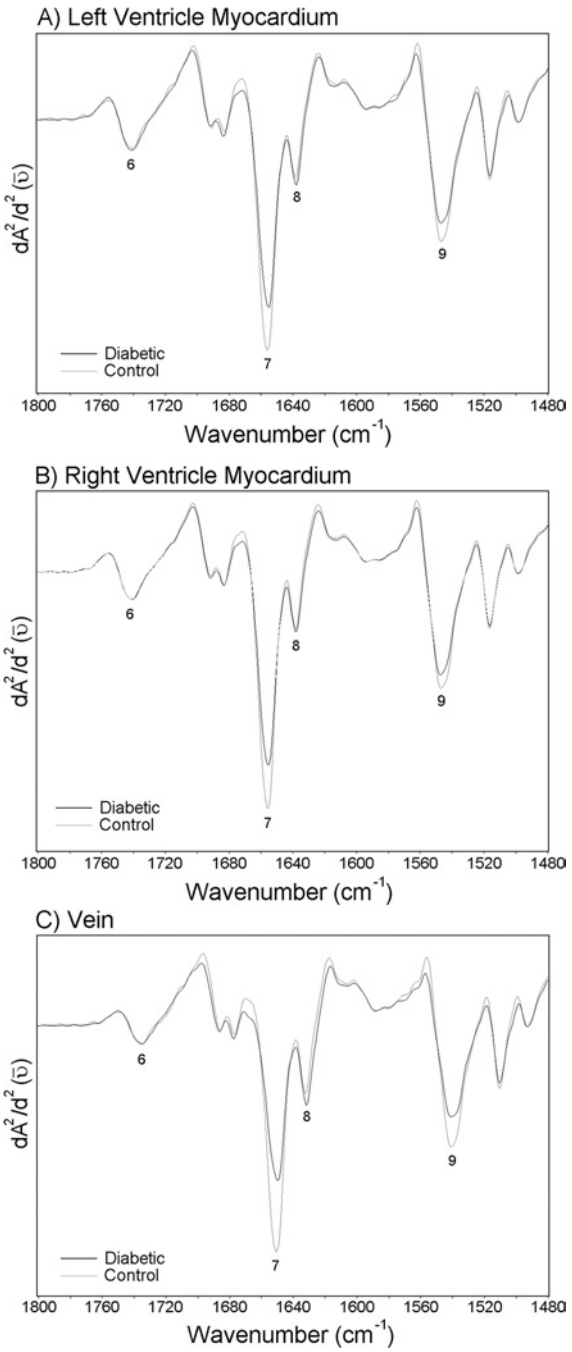

Figure 4 Average spectra belonging to the left ventricle myocardium, the right ventricle myocardium and the vein of the control and the diabetic groups in the 1480–1800 cm^{-1} region

Vector normalization was done in the 950–1480 cm^{-1} region. Absorption maxima appear as minima in the second derivatives. (**A**) Second derivative average spectra belonging to the left ventricle myocardium; (**B**) second derivative average spectra belonging to the right ventricle myocardium; (**C**) second derivative average spectra belonging to the vein.

Table 4 Changes in the intensities of the main functional groups in the 1480–1800 cm^{-1} region for control and diabetic groups

Data are given as means ± S.D. $P \leqslant 0.05$ were accepted as significantly different from the control group.

	Left ventricle myocardium			Right ventricle myocardium			Vein		
Functional groups	Control	Diabetic	*P* values	Control	Diabetic	*P* values	Control	Diabetic	*P* values
Amide I: α-helical structure (at 1655 cm^{-1})	−0.830 ± 0.065	−0.680 ± 0.100	⩽0.01	−0.926 ± 0.089	−0.756 ± 0.069	⩽0.001	−0.730 ± 0.068	−0.510 ± 0.035	⩽0.001
Amide I: β-sheet structure (at 1638 cm^{-1})	−0.210 ± 0.011	−0.240 ± 0.010	⩽0.01	−0.224 ± 0.017	−0.237 ± 0.010		−0.220 ± 0.019	−0.260 ± 0.024	⩽0.01
Amide II: α-helical structure (at 1545 cm^{-1})	−0.420 ± 0.024	−0.358 ± 0.032	⩽0.01	−0.430 ± 0.035	−0.390 ± 0.027	⩽0.01	−0.380 ± 0.022	−0.280 ± 0.036	⩽0.001

structures and the band at 1637 cm^{-1} is attributable to Amide I of β-sheet structures. It is possible to see another band in the same Figure located around 1548 cm^{-1}, which arises from the Amide II of α-helical structures of proteins [24]. As seen in Figure 4 and Table 4, diabetes causes a significant decrease in the intensities of α-helix of Amide I and Amide II bands, and causes a remarkable increase in the intensity of β-sheet of Amide I band.

The 1000–1270 cm^{-1} region

The spectral region 1000–1300 cm^{-1} is mainly shaped by PO_2^- stretching modes, and the C–O stretching modes of various oligo- and poly-saccharides [29]. The average spectra belonging to the left ventricle myocardium, the right ventricle myocardium and the vein of the control and diabetic groups in the 1000–1270 cm^{-1} region are given in Figure 5. The main changes in the intensity values of the investigated functional groups are given in Table 5. Figure 5 clearly shows a band at 1201 cm^{-1} (marked with an arrow in the Figure) only in the vein spectra, which arises due to the collagen present in the system [24]. Actually, the types of collagen exhibit a series of absorptions between 1000 and 1300 cm^{-1}, which arise from the C–O stretching vibrations of the carbohydrate moieties attached to proteins and the C–N stretching vibrations of the collagen amide backbone. The efficacy of the 1201 cm^{-1} band for accurate identification of cardiac collagen deposition was demonstrated in a previous study [21] by correlating the results obtained using trichrome staining and IR microscopic mapping of collagen. For this reason, in the present study, we used the band at 1201 cm^{-1} as the represented band for collagen. Our results revealed an apparent increase (from -0.009 ± 0.006 to $-0.021 \pm 0.007^{**}$; the double asterisk indicates that the degree of significance between the control and the diabetic vein was $P \leqslant 0.01$) in the intensity of this collagen band in diabetic vein. This might be due to an increase in the content of collagen. The band at 1151 cm^{-1} is a C–O stretching band arising due to the presence of glycogen in the system [29,30], and the band giving an absorption at 1171 cm^{-1} is due to CO–O–C asymmetric stretching arising from ester bonds in cholesteryl esters and phospholipids [29]. The ratio of the intensities of the absorptions at 1151 and 1171 cm^{-1} is reversed in all the diabetic groups. The other band in the spectrum of diabetic group in which we see an increase in the intensity value gives an absorption peak at 1083 cm^{-1}. This band can be assigned as the PO_2^- symmetric stretching band arising from phospholipids [31] or due to the C–O stretching band which mainly arises from glycogen, oligosaccharides and glycolipids present in the system [29,32]. Figure 5 also illustrates the presence of a sharp band at 1041 cm^{-1}, originating from the various C–O stretching vibrations characteristic for polysaccharides [33]. It is possible to observe a slight increase in the intensity of this band in all the diabetic groups.

DISCUSSION

It is known that the dominant lipid bands in the 2800–3030 cm^{-1} region originate from the C–H stretching vibrations of the fatty acyl chains of membrane lipids [32]. The intensity or area of IR absorptions arising from a particular species is directly proportional to the concentration of that species [34]. It is seen in Figure 3 that a significant increase in the intensity of the band occurs at 3012 cm^{-1}, which was assigned as olefinic=CH band in the average spectrum of the vein in the diabetic group. The intensity of the olefinic=CH band can be used as an index of relative concentration of double bonds in the lipid structure of unsaturated lipids [28,35]. The increase in the intensity of this band in the diabetic vein with respect to the control suggests that DM might be causing an increase in the concentration of unsaturated fatty acids in veins of the left ventricle myocardium. This result is in agreement with previous studies, one of which showed that the content of double bonds (=CH) in diabetic platelets increases, suggesting a higher lipid peroxidation in these platelets [32]. In another study, an increase in the area of this band of diabetic rat liver microsomal membranes was reported [35]. These double bonds mainly originate from lipid peroxidative end-products, such as malondialdehyde. Consequently, it is possible to deduce in our study that there is a slightly increased peroxidative process in the veins. On the other hand, our result is in contradiction with a previous study that demonstrated that STZ-induced diabetes decreases the content of this functional group [36].

As seen in Figure 3 and Table 2, the intensities of the CH_2 symmetric and asymmetric stretching bands increase significantly in the left ventricle myocardium and the vein of the diabetic group, which corresponds to an increase in the lipid content; whereas the content of CH_3 groups decreases in the diabetic group with respect to the control. In the right ventricle myocardium, the changes observed in the contents of these functional groups show the same trend, but the changes in the content of the CH_3 symmetric and asymmetric and CH_2 asymmetric stretching modes are less significant than those of the left ventricle myocardium and the vein. As demonstrated in Table 3, the lipid/protein ratio increases in all the investigated regions of the diabetic heart. This increase in the ratio can be due to an increase in the lipid content and/or a decrease in the protein content. The increase in lipid content might be due to the disturbance of lipid metabolism in diabetic ventricle myocardium and the vein. Supporting our observations, an increase in lipid content and a strong correlation between elevated levels of lipid and the decrease in the heart

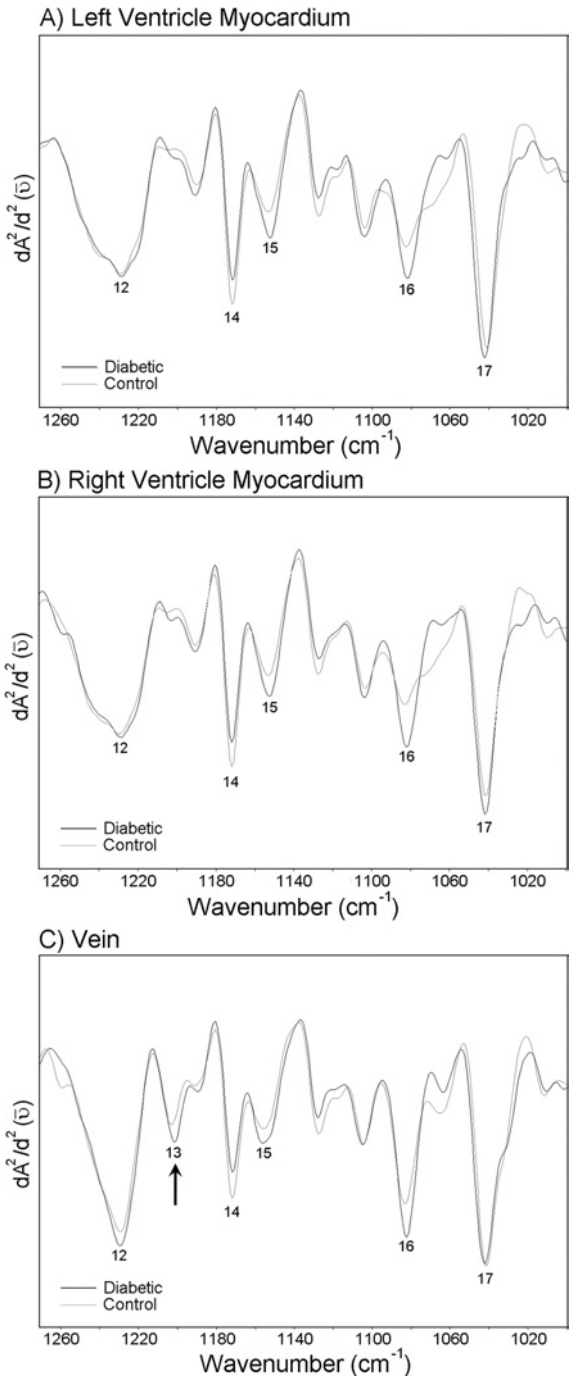

Figure 5 Average spectra belonging to the left ventricle myocardium, the right ventricle myocardium and the vein of the control and the diabetic groups in the 1000–1270 cm^{-1} region

Vector normalization was done in the 950–1480 cm^{-1} region. Absorption maxima appear as minima in the second derivatives. (**A**) Second derivative average spectra belonging to the left ventricle myocardium; (**B**) second derivative average spectra belonging to the right ventricle myocardium; (**C**) second derivative average spectra belonging to the vein.

function was demonstrated in previous studies [37,38]. It was reported in another previous study that in rats which were diabetic for 16 weeks, the mitochondria was damaged so severely that it no longer could metabolize cardiac lipid properly, resulting in the breakdown of the mitochondria and accumulation of lipids [8]. In our study, even though the rats were diabetic only for 5 weeks, there is a lipid accumulation in the myocardium, which might be an indication for the damage of mitochondria. Accumulation of fatty acids and their metabolites, such as long-chain acyl-CoA and long-chain acyl-carnitine, has been associated with cardiac dysfunction and cell damage in diabetic hearts. Alterations in the composition of membrane phospholipids are also considered to change the activities of various membrane-bound enzymes and subsequently heart function under different pathophysiological conditions [39].

Diabetes causes a decrease in the content of α-helical structure of the diabetic heart, more significantly in the vein (Figure 4 and Table 4). Diabetes causes an increase in the concentration of β-sheet structure, more significantly in the left ventricle myocardium and the vein (Figure 4 and Table 4). Thus we can deduce that DM might be causing some important structural changes in the proteins of the diabetic heart. In a previous study, it was shown that, in diabetes, proteins exposed to glucose are cleaved, undergo conformational changes and develop fluorescent adducts [40]. These changes were presumed to result from the covalent attachment of glucose to amino groups. Glycated proteins may be rearranged to AGEs (advanced glycation end-products), which also contribute to the development of diabetic complications [41]. Binding of AGEs to their receptors can lead to modification in cell signalling and further production of free radicals [42].

As demonstrated in Figure 5, there is an apparent increase in the content of collagen in the diabetic vein. A pure collagen spectrum is presented in Figure 6, as an example. In this pure spectrum, an absorption peak is observed at 1203 cm^{-1} (pointed with an arrow), which is similarly located as the peak we have observed in the vein spectrum as demonstrated in Figure 5. In the literature, there is evidence from *in vitro* studies that diabetes exerts an influence both on cell growth and on the composition of the extracellular matrix, with an increase in collagen component [43]. The band at 1151 cm^{-1} is a C–O stretching band arising due to the presence of glycogen in the system [29,30], and the band giving an absorption peak at 1171 cm^{-1} is a CO–O–C asymmetric stretching band arising from ester bonds in cholesteryl esters and phospholipids [29], as mentioned previously. A pure glycogen spectrum from rabbit liver is demonstrated in Figure 7. In this pure spectrum, two absorption peaks are observed at 1081 and 1152 cm^{-1} (indicated by arrows), with similar locations to the peaks we have observed in the spectra given in Figure 5. The increase in the intensity of the band at 1151 cm^{-1} in the diabetic group might be due to an increase in the content of glycogen. It is believed that, in the diabetic heart, high levels of plasma non-esterified fatty acids cause glycogen accumulation [39], which might be due to the disturbance of carbohydrate and lipid metabolism. It is clearly demonstrated in Figure 5 and Table 5 that the ratio of the intensities of the absorptions at 1151 and 1171 cm^{-1} is reversed in the diabetic groups of all the investigated parts of the heart, meaning that the intensity of the band at 1151 cm^{-1} increased and the intensity of the band at 1171 cm^{-1} decreased in the diabetic group with respect to the control. This type of change in the intensity ratio of these bands was previously observed in the infarcted heart [24]. Hence, it is possible to deduce that DM causes similar changes to the infarction on the heart. The other band in the diabetic group in which we see an increase in the intensity gives an absorption peak at 1083 cm^{-1}. This increase might be due to an increase in the lipid and/or glycolipid and/or glycogen contents. The major contribution to the intensity of this band might be due to the presence of a large amount of glycogen within the cytoplasm of Purkinje fibres in the cardiac tissue. It is important to note that the intensity of the bands at 1080, 1156 and 1228 cm^{-1} could also have arisen due to the DNA of the rat heart [44,45]. Figure 5 illustrates the presence of a sharp band at

Table 5 Changes in the intensities of the main functional groups in the 1000–1270 cm^{-1} region for control and diabetic groups

Data are given as means ± S.D. $P \leqslant 0.05$ were accepted as significantly different from the control group.

	Left ventricle myocardium			Right ventricle myocardium			Vein		
Functional groups	Control	Diabetic	*P* values	Control	Diabetic	*P* values	Control	Diabetic	*P* values
CO–O–C asym. stretching (at 1173 cm^{-1})	−0.061 ± 0.003	−0.049 ± 0.008	⩽0.05	−0.062 ± 0.004	−0.049 ± 0.006	⩽0.001	−0.047 ± 0.004	−0.033 ± 0.005	⩽0.001
C–O stretching (at 1151 cm^{-1})	−0.012 ± 0.002	−0.026 ± 0.004	⩽0.001	−0.013 ± 0.004	−0.023 ± 0.006	⩽0.01	−0.009 ± 0.005	−0.018 ± 0.004	⩽0.01
C–O stretching/CO–O–C asym. stretching	0.197 ± 0.040	0.546 ± 0.162	⩽0.001	0.210 ± 0.060	0.490 ± 0.170	⩽0.001	0.195 ± 0.127	0.530 ± 0.187	⩽0.01
PO_2^- sym. stretching (at 1080–1085 cm^{-1})	−0.031 ± 0.003	−0.047 ± 0.012	⩽0.01	−0.029 ± 0.004	−0.052 ± 0.012	⩽0.01	−0.050 ± 0.006	−0.070 ± 0.008	⩽0.001
C–O stretching (at 1041 cm^{-1})	−0.084 ± 0.005	−0.089 ± 0.014		−0.078 ± 0.015	−0.090 ± 0.009	⩽0.05	−0.083 ± 0.012	−0.080 ± 0.056	

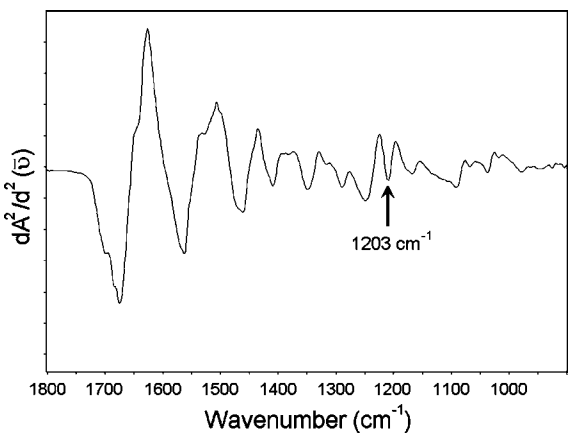

Figure 6 IR spectrum belonging to Type I collagen

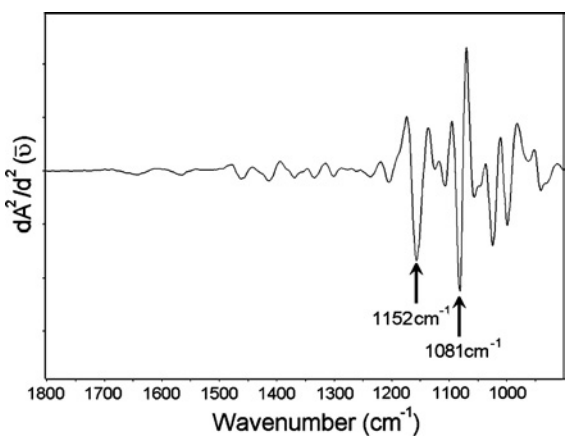

Figure 7 IR glycogen spectrum from rabbit liver (dry film)

1041 cm^{-1}, originating from the various C–O stretching vibrations characteristic for oligosaccharides and polysaccharides. It is possible to observe a slight increase in the concentration of this functional group in diabetic samples, implying that diabetes might be causing oligo- and poly-saccharide accumulation.

By considering the results of both ventricle myocardia and the vein of the heart, an apparent increase in the content of lipids was observed. In previous studies, an increase in triacylglycerols and cholesterol in rat myocardium was reported after 8 weeks of diabetes [24]. In our study, we see an increase in the lipid content even after 5 weeks of diabetes. The findings of our study are important in this aspect since they reveal that lipid metabolism is altered at early onset of diabetes. This increase in the lipid content might lead to cardiomyopathy in diabetes, as suggested by others [46–48].

Conclusion

Despite the dramatic improvement in diagnostic procedures and treatment of diabetic patients, cardiovascular complications are still the most frequent causes of death in these patients. Thus the study of heart disease in diabetic patients is of great clinical importance.

Some of the studies in the literature show that the left ventricle is seriously affected by diabetes, whereas some of the others demonstrate that the right ventricle is more severely affected. In most of the previous studies, the right ventricle was not even evaluated, partly because only the left ventricle was subject to the primary haemodynamic overload, and the pathological processes were expected to primarily involve the left ventricle. Study of mechanisms of biventricular pathology may provide insight into the pathogenesis of ventricular damage and subsequent heart failure.

Our findings suggest that DM causes some alterations that may contribute to the development of cardiac and cardiovascular disease in diabetes. The main common effects are: increase in lipid content and increase in glycogen and glycolipid contents. Additionally, we for the first time showed an altered protein profile with a decrease in α-helix and an increase in β-sheet structure in all the diabetic groups. In previously published papers [7,8,11,12,21,24,32], the effect of diabetes on hearts of animals and/or humans that were diabetic for long periods of time (mostly from 2 months to 10 years) had been investigated. The present study demonstrates that even a relatively short term (5 weeks) of diabetes induces significant effects, as mentioned above, on both ventricle myocardia of the rat heart including the vein.

This work was supported by TÜBİTAK (Scientific and Technical Research Council of Turkey): BAYG (Directorate of Human Resources Development) and BAP-(AFP)-2001-07-02-00-48.

REFERENCES

1 Kakkar, R., Mantha, S. V., Kalra, J. and Prasad, K. (1996) Time course study of oxidative stress in aorta and heart of diabetic rat. Clin. Sci. (Lond.) **91**, 441–448

2 Barbano, R., Hart-Gouleau, S., Pennella-Vaughan, J. and Dworkin, R. H. (2003) Pharmacotherapy of painful diabetic neuropathy. Curr. Pain Headache Rep. **7**, 169–177
3 Prasad, S., Kamath, G. G., Jones, K., Clearkin, L. G. and Phillips, R. P. (2001) Prevalence of blindness and visual impairment in a population of people with diabetes. Eye **15**, 640–643
4 Iyoda, M., Kuroki, A., Kato, K., Kato, N., Hirano, T. and Sugisaki, T. (2003) A case of acute renal failure due to rhabdomyolysis associated with non-autoimmune fulminant type IB diabetes mellitus. Clin. Nephrol. **59**, 301–304
5 Herrman, C. E., Sanders, R. A., Klaunig, J. E., Schwarz, L. R. and Watkins, III, J. B. (1999) Decreased apoptosis as a mechanism for hepatomegaly in streptozotocin-induced diabetic rats. Toxicol. Sci. **50**, 146–151
6 Panzram, G. (1987) Mortality and survival in type 2 (non-insulin-dependent) diabetes mellitus. Diabetologia **30**, 123–131
7 Grossman, E. and Messerli, F. H. (1996) Diabetic and hypertensive heart disease. Ann. Intern. Med. **125**, 304–310
8 Hsiao, Y. C., Suzuki, K., Abe, H. and Toyota, T. (1987) Ultrastructural alterations in cardiac muscle of diabetic BB Wistar rats. Virchows Arch. A Pathol. Anat. Histopathol. **411**, 45–52
9 Factor, S. M., Minase, T. and Sonnenblick, E. H. (1980) Clinical and morphological features of human hypertensive-diabetic cardiomyopathy. Am. Heart J. **99**, 446–458
10 Litwin, S. E., Raya, T. E., Anderson, P. G., Daugherty, S. and Goldman, S. (1990) Abnormal cardiac function in the streptozotocin-diabetic rat. Changes in active and passive properties of the left ventricle. J. Clin. Invest. **86**, 481–488
11 Doi, K., Sawada, F., Toda, G., Yamachika, S., Seto, S., Urata, Y., Ihara, Y., Sakata, N., Taniguchi, N., Kondo, T. and Yano, K. (2001) Alteration of antioxidants during the progression of heart disease in streptozotocin-induced diabetic rats. Free Radical Res. **34**, 251–261
12 Factor, S. M., Borczuk, A., Charron, M. J., Fein, F. S., van Hoeven, K. H. and Sonnenblick, E. H. (1996) Myocardial alterations in diabetes and hypertension. Diabetes Res. Clin. Pract. **31**, S133–S142
13 Parinandi, N. L., Thompson, E. W. and Schmid, H. H. (1990) Diabetic heart and kidney exhibit increased resistance to lipid peroxidation. Biochim. Biophys. Acta **1047**, 63–69
14 Factor, S. M., Okun, E. M. and Minase, T. (1980) Capillary microaneurysms in the human diabetic heart. N. Engl. J. Med. **302**, 384–388
15 Hamby, R. I., Zoneraich, S. and Sherman, L. (1974) Diabetic cardiomyopathy. JAMA, J. Am. Med. Assoc. **229**, 1749–1754
16 Fein, F. S. and Sonnenblick, E. H. (1985) Diabetic cardiomyopathy. Prog. Cardiovasc. Dis. **27**, 255–270
17 Silver, M. D., Huckell, V. F. and Lorber, M. (1977) Basement membranes of small cardiac vessels in patients with diabetes and myxoedema: preliminary observations. Pathology **9**, 213–220
18 Lewis, R. N. A. H. and McElhaney, R. N. (1996) Fourier transform infrared spectroscopy in the study of hydrated lipids and lipid bilayer membranes. In Infrared Spectroscopy of Biomolecules (Mantsch, H. H. and Chapman, D., eds.), pp. 159–202, Wiley-Liss, New York
19 Lester, D. S., Kidder, L. H., Levin, I. W. and Lewis, E. N. (1998) Infrared microspectroscopic imaging of the cerebellum of normal and cytarabine treated rats. Cell. Mol. Biol. (Noisy-le-grand) **44**, 29–38
20 LeVine, S. M., Radel, J. D., Sweat, J. A. and Wetzel, D. L. (1999) Microchemical analysis of retina layers in pigmented and albino rats by Fourier transform infrared microspectroscopy. Biochim. Biophys. Acta **1473**, 409–417
21 Liu, K. Z., Dixon, I. M. and Mantsch, H. H. (1999) Distribution of collagen deposition in cardiomyopathic hamster hearts determined by infrared microscopy. Cardiovasc. Pathol. **8**, 41–47
22 Bohic, S., Heymann, D., Pouezat, J. A., Gauthier, O. and Daculsi, G. (1998) Transmission FT-IR microspectroscopy of mineral phases in calcified tissues. C. R. Acad. Sci. III **321**, 865–876
23 Kneipp, J., Lasch, P., Baldauf, F., Beekes, M. and Naumann, D. (2000) Detection of pathological molecular alterations in scrapie-infected hamster brain by Fourier transform infrared (FT-IR) spectroscopy. Biochim. Biophys. Acta **1501**, 189–199
24 Liu, K., Jackson, M., Sowa, M. G., Ju, H., Dixon, I. M. and Mantsch, H. H. (1996) Modification of the extracellular matrix following myocardial infarction monitored by FTIR spectroscopy. Biochim. Biophys. Acta **1315**, 73–77
25 Kneipp, J., Miller, L. M., Joncic, M., Kittel, M., Lasch, P., Beekes, M. and Naumann, D. (2003) *In situ* identification of protein structural changes in prion-infected tissue. Biochim. Biophys. Acta **1639**, 152–158
26 Yoshida, S. and Yoshida, H. (2004) Noninvasive analyses of polyunsaturated fatty acids in human oral mucosa *in vivo* by Fourier-transform infrared spectroscopy. Biopolymers **74**, 403–412
27 Choo, L.-P., Wetzel, D. L. B., Halliday, W. C., Jackson, M., LeVine, S. M. and Mantsch, H. H. (1996) *In situ* characterization of L-amyloid in Alzheimer's diseased tissue by Synchrotron Fourier transform infrared microspectroscopy. Biophys. J. **71**, 1672–1679
28 Takahashi, H., French, S. W. and Wong, P. T. (1991) Alterations in hepatic lipids and proteins by chronic ethanol intake: a high-pressure Fourier transform infrared spectroscopic study on alcoholic liver disease in the rat. Alcohol. Clin. Exp. Res. **15**, 219–223
29 Jackson, M., Ramjiawan, B., Hewko, M. and Mantsch, H. H. (1998) Infrared microscopic functional group mapping and spectral clustering analysis of hypercholesterolemic rabbit liver. Cell. Mol. Biol. (Noisy-ie-grand) **44**, 89–98
30 Diem, M., Boydston-White, S. and Chiriboga, L. (1999) Infrared spectroscopy of cells and tissues: Shining light onto a novel subject. Appl. Spectrosc. **53**, 148a–161a
31 Manoharan, R., Baraga, J. J., Rava, R. P., Dasari, R. R., Fitzmaurice, M. and Feld, M. S. (1993) Biochemical analysis and mapping of atherosclerotic human artery using FT-IR microspectroscopy. Atherosclerosis **103**, 181–193
32 Liu, K. Z., Bose, R. and Mantsch, H. H. (2002) Infrared spectroscopic study of diabetic platelets. Vib. Spectrosc. **28**, 131–136
33 Lyman, D. J. and Murray-Wijelath, J. (1999) Vascular graft healing: I. FTIR analysis of an implant model for studying the healing of a vascular graft. J. Biomed. Mater. Res. **48**, 172–186
34 Dubois, J., Baydack, R., McKenzie, E., Booth, T. and Jackson, M. (2003) Scrapie infection investigated by magnetic resonance imaging and Fourier transform infrared microscopy. Vib. Spectrosc. **32**, 95–105
35 Severcan, F., Gorgulu, G., Gorgulu, S. T. and Guray, T. (2005) Rapid monitoring of diabetes-induced lipid peroxidation by Fourier transform infrared spectroscopy: evidence from rat liver microsomal membranes. Anal. Biochem. **339**, 36–40
36 Sills, R. H., Moore, D. J. and Mendelsohn, R. (1994) Erythrocyte peroxidation: quantitation by Fourier transform infrared spectroscopy. Anal. Biochem. **218**, 118–123
37 Heyliger, C. E., Rodrigues, B. and McNeill, J. H. (1986) Effect of choline and methionine treatment on cardiac dysfunction of diabetic rats. Diabetes **35**, 1152–1157
38 McNeill, J. H. (1996) Role of elevated lipids in diabetic cardiomyopathy. Diabetes Res. Clin. Pract. **31**, S67–S71
39 Dhalla, N. S., Elimban, V. and Rupp, H. (1992) Paradoxical role of lipid metabolism in heart function and dysfunction. Mol. Cell. Biochem. **116**, 3–9
40 Kugiyama, K., Kems, S. A., Morrisett, J. D., Roberts, R. and Henry, P. D. (1990) Impairment of endothelium-dependent arterial relaxation by lysolecithin in modified low-density lipoproteins. Nature (London) **344**, 160–162
41 Maxwell, S. R. and Lip, G. Y. (1997) Free radicals and antioxidants in cardiovascular disease. Br. J. Clin. Pharmacol. **44**, 307–317
42 Penckofer, S., Schwertz, D. and Florczak, K. (2002) Oxidative stress and cardiovascular disease in type 2 diabetes: the role of antioxidants and pro-oxidants. J. Cardiovasc. Nurs. **16**, 68–85
43 Turk, Z., Misur, I., Turk, N. and Benko, B. (1999) Rat tissue collagen modified by advanced glycation: correlation with duration of diabetes and glycemic control. Clin. Chem. Lab. Med. **37**, 813–820
44 Liquier, J. and Taillandier, R. (1996) Infrared spectroscopy of nucleic acids. In Infrared Spectroscopy of Biological Molecules (Mantsch, H. H. and Chapman, D., eds.), pp. 131–158, Wiley-Liss, New York
45 Cakmak, G., Togan, I., Uguz, C. and Severcan, F. (2003) FT-IR spectroscopic analysis of rainbow trout liver exposed to nonylphenol. Appl. Spectrosc. **57**, 835–841
46 Rodrigues, B., Cam, M. C. and McNeill, J. H. (1995) Myocardial substrate metabolism: implications for diabetic cardiomyopathy. J. Mol. Cell. Cardiol. **27**, 169–179
47 Lopaschuk, G. D. (1996) Fatty acid metabolism in the heart following diabetes. In The Heart in Diabetes (Chatman, J. C., Phil, D., Forder, J. R. and McNeill, J. H., eds.), pp. 215–251, Kluwer Academic Publishers, Boston, MA
48 Matsui, H., Okumura, K., Mukawa, H., Hibino, M., Toki, Y. and Ito, T. (1997) Increased oxysterol contents in diabetic rat hearts: their involvement in diabetic cardiomyopathy. Can. J. Cardiol. **13**, 373–379
49 Toyran, N., Zorlu, F., Donmez, G., Oge, K. and Severcan, F. (2004) Chronic hypoperfusion alters the content and structure of proteins and lipids of rat brain homogenates: a Fourier transform infrared spectroscopy study. Eur. Biophys. J. **33**, 549–554
50 Severcan, F., Toyran, N., Kaptan, N. and Turan, B. (2000) Fourier transform infrared study of the effect of diabetes on rat liver and heart tissues in the C–H region. Talanta **53**, 55–59

Received 30 January 2006/5 April 2006; accepted 12 April 2006
Published as BJ Immediate Publication 12 April 2006, doi:10.1042/BJ20060171